Control of Formation and Dissociation of the High-Affinity Complex between Cytochrome *c* and Cytochrome *c* Peroxidase by Ionic Strength and the Low-Affinity Binding Site†

Hongkang Mei,‡ Kefei Wang,‡ Stacey McKee,‡ Xuming Wang,§ Jennifer L. Waldner,§ Gary J. Pielak,§ Bill Durham,‡ and Francis Millett*,‡

Department of Chemistry and Biochemistry, University of Arkansas, Fayetteville, Arkansas 72701, and Departments of Chemistry and Biochemistry and Biophysics, University of North Carolina, Chapel Hill, North Carolina 27599-3290

Received June 21, 1996; Revised Manuscript Received October 14, 1996⊗

ABSTRACT: A new ruthenium photoreduction technique was used to measure the formation and dissociation rate constants k_f and k_d of the high-affinity complex between yeast iso-1-cytochrome *c* (yC*c*) and cytochrome *c* peroxidase compound I (CMPI) over a wide range of ionic strength. These studies utilized Ru-39-C*c*, which contains trisbipyridylruthenium attached to the cysteine residue in the H39C,C102T variant of yC*c*, and has the same reactivity with CMPI as native yC*c*. k_d and k_f were measured by photoreducing a small concentration of Ru-39-C*c* in the presence of the oxidized yCc^{III}:CMPI complex, which must dissociate before Ru-39-Cc^{II} can bind to CMPI and reduce the radical cation. The value of k_d for the 1:1 high-affinity complex is very small at low ionic strength, <5 s^{-1} but is increased significantly by binding yC*c* to a second low-affinity site. However, the low-affinity yC*c* binding site is not active in direct electron transfer to either the radical cation or the oxyferryl heme in CMPI, and is too weak to play a role in the kinetics at ionic strengths above 70 mM. The value of k_d increases to 4000 s^{-1} at 150 mM ionic strength, while k_f decreases from $>3 \times 10^9$ M^{-1} s^{-1} at low ionic strength to 1.3×10^9 M^{-1} s^{-1} at 150 mM ionic strength. These studies indicate that the rate-limiting step in enzyme turnover is product dissociation below 150 mM ionic strength and intracomplex electron transfer to the oxyferryl heme at higher ionic strength. The interaction between yC*c* and C*c*P is optimized at physiological ionic strength to provide the largest possible complex formation rate constant k_f without allowing product dissociation to be rate-limiting. The effects of surface mutations on the kinetics provided evidence that the high-affinity binding site used for the reaction in solution is similar to the one identified in the yC*c*:C*c*P crystal structure.

Electron transfer reactions between metalloproteins are difficult to characterize in detail because they are dependent on so many different factors, including the kinetics of complex formation and dissociation, the distance and pathway for electron transfer, and the driving force and reorganization energy of the reaction. The reaction between cytochrome *c* (C*c*)[1] and cytochrome *c* peroxidase (C*c*P) has become an important testing ground for characterizing each of these factors. The resting ferric state of C*c*P is oxidized by hydrogen peroxide to CMPI(Fe^{IV}=O,$Trp^{\bullet+}$), which contains an oxyferryl heme Fe^{IV}=O and a radical cation located on the indole group of Trp-191 (Mauro et al., 1988; Scholes et al., 1989; Erman et al., 1989; Sivaraja et al., 1989; Miller et al., 1994a; Fitzgerald et al., 1994; Huyett et al., 1995). Hahm et al. (1994) and Liu et al. (1994) have proposed a mechanism for the sequential reduction of CMPI to C*c*P by two molecules of Cc^{II}, as shown in Scheme 1.

Scheme 1

$$\text{CMPI}(Fe^{IV}{=}O,Trp^{\bullet+}) + Cc^{II} \rightarrow \text{CMPII}(Fe^{IV}{=}O,Trp) + Cc^{III}$$

$$\text{CMPII}(Fe^{IV}{=}O,Trp) + 2H^{+} \rightleftarrows \text{CMPII}(Fe^{III},Trp^{\bullet+}) + H_2O$$

$$\text{CMPII}(Fe^{III},Trp^{\bullet+}) + Cc^{II} \rightarrow Cc\text{P}(Fe^{III},Trp) + Cc^{III}$$

A substantial body of evidence supports the initial reduction of the Trp-191 radical cation in CMPI(Fe^{IV}=O,$Trp^{\bullet+}$) by Cc^{II} (Geren et al., 1991; Hahm et al., 1992, 1993, 1994; Roe & Goodin, 1993; Liu et al., 1994, 1995; Miller et al, 1994b, 1995, 1996; Wang et al., 1996). CMPII(Fe^{IV}=O,Trp) is converted to CMPII(Fe^{III},$Trp^{\bullet+}$) by internal electron transfer from Trp-191 to the oxyferryl heme, and Cc^{II} then reduces the radical cation to form C*c*P. The equilibrium constant for the conversion of CMPII(Fe^{IV}=O,Trp) to CMPII(Fe^{III},$Trp^{\bullet+}$) is dependent on pH and strongly favors CMPII(Fe^{IV}=O,Trp) at pH 7 and above (Coulson et al., 1971; Liu et al., 1994). An alternative mechanism involving initial reduction of the oxyferryl heme has been proposed by Matthis & Erman (1995) and Matthis et al. (1995). A

† This work was supported in part by NIH Grants GM20488 to B.D. and F.M. and GM42501 to G.P.

‡ University of Arkansas.

§ University of North Carolina.

⊗ Abstract published in *Advance ACS Abstracts,* November 15, 1996.

[1] Abbreviations: C*c*, cytochrome *c*; hC*c*, horse C*c*; yC*c*, yeast iso-1-C*c*; C*c*P, cytochrome *c* peroxidase; CMPI, C*c*P compound I; Ru-39-yC*c*, Ru(bpy)$_2$(4,4′-dimethylbipyridine-Cys-39-yeast-iso-1-cytochrome *c*); MPB, 3-(*N*-maleimidiylpropionyl)biocytin; ^{3}ZnC*c*, photoexcited triplet state of Zn-porphyrin-C*c*.

S0006-2960(96)01487-0 CCC: $12.00

comparison between the two mechanisms is discussed by Wang et al. (1996).

Each of the interprotein electron transfer reactions shown in Scheme 1 requires at least three steps, formation of a transient reactant complex between the two proteins, electron transfer within the reactant complex to form a product complex, and dissociation of the product complex. Therefore, complete reduction of CMPI by two molecules of C*c*^{II} can be described by the minimal mechanism shown in Scheme 2, in which I, II, and E represent CMPI, CMPII,

Scheme 2

$$\mathrm{I} + \mathrm{C}c^{\mathrm{II}} \underset{k_d}{\overset{k_f}{\rightleftharpoons}} \mathrm{I{:}C}c^{\mathrm{II}} \xrightarrow{k_{eta}} \mathrm{II{:}C}c^{\mathrm{III}} \underset{k_f}{\overset{k_d}{\rightleftharpoons}} \mathrm{II} + \mathrm{C}c^{\mathrm{III}}$$

$$\mathrm{II} + \mathrm{C}c^{\mathrm{II}} \underset{k_d}{\overset{k_f}{\rightleftharpoons}} \mathrm{II{:}C}c^{\mathrm{II}} \xrightarrow{k_{etb}} \mathrm{E{:}C}c^{\mathrm{III}} \underset{k_f}{\overset{k_d}{\rightleftharpoons}} \mathrm{E} + \mathrm{C}c^{\mathrm{III}}$$

and C*c*P, respectively. The rate-limiting step in Scheme 2 can be complex formation, complex dissociation, or one of the intracomplex electron transfer steps, depending on experimental conditions.

Scheme 2 is based on the assumption that C*c* binds to a high-affinity site on CMPI to form a 1:1 complex. However, Kang et al. (1977) and Kornblatt and English (1986) have shown that a second molecule of C*c* can bind to a low-affinity site on C*c*P to form a 2:1 complex. The binding of C*c* to the low-affinity binding site appears to affect the steady-state kinetics at low ionic strength (Matthis et al., 1995; Miller et al., 1996), but the mechanism by which it does so is not clear. Stemp and Hoffman (1993) and Zhou and Hoffman (1993, 1994) found that the low-affinity site is active in electron transfer in 2:1 complexes between yC*c* and Zn-porphyrin C*c*P, and between Zn-porphyrin-hC*c* and ferric C*c*P. However, it was not possible to study the CMPI state with this method, and so it is not known whether the low-affinity binding site is active in electron transfer to either the oxyferryl heme or the Trp-191 indolyl radical cation.

Wang et al. (1996) recently designed a new yeast Ru-C*c* derivative, Ru-39-C*c*, to measure the rate constants for intracomplex electron transfer to the radical cation and the oxyferryl heme, $k_{eta} = 2 \times 10^6$ s^{-1} and $k_{etb} = 5000$ s^{-1}. In the present paper we describe a new method to measure the formation and dissociation rate constants k_f and k_d over a wide range of ionic strength. The role of the low-affinity C*c* binding site in electron transfer and complex dissociation is also studied by this method. The location of the binding domain used for reduction of both the radical cation and the oxyferryl heme is determined using a series of surface charge mutants of C*c*P.

EXPERIMENTAL PROCEDURES

Materials. Yeast iso-1-C*c* was obtained from Sigma Chemical Co. and purified as described by Miller et al. (1994b). Ru-39-C*c* was prepared as described by Geren et al. (1995). CMPI(MI) and the mutants E32Q, D34N, E35N, E290N, E291Q, and A193F were prepared as described by Fishel et al. (1987) and Miller et al. (1994b).

Laser Flash Photolysis Studies. Flash photolysis studies were carried out as described by Geren et al. (1991). The excitation flash was provided by a Phase R model DL 1400 flash lamp-pumped dye laser producing a 450 nm light flash with <0.5 μs duration. The probe source was a tungsten lamp. The flash photolysis experiments were carried out in glass semimicro cuvettes containing 300 μL solutions of 2 mM sodium phosphate, pH 7.0, 0−300 mM NaCl, 1−50 μM Ru-39-C*c*, and 1−20 μM CMPI. The reduction and reoxidation of the Ru-39-C*c* heme was measured at 550 nm, while the reduction of the oxyferryl heme in CMPII was measured at 434 nm. The concentration of photoreduced Ru-39-Cc^{II} was always less than 5% of [CMPI], and pseudo-first-order kinetics were obeyed. The experimental transients were fitted with a single exponential equation using the OLIS KINFIT program to obtain k_{obs}. The error limits for k_{obs} given in the figures and text represent 95% confidence limits obtained from at least three independent measurements.

Scheme 3

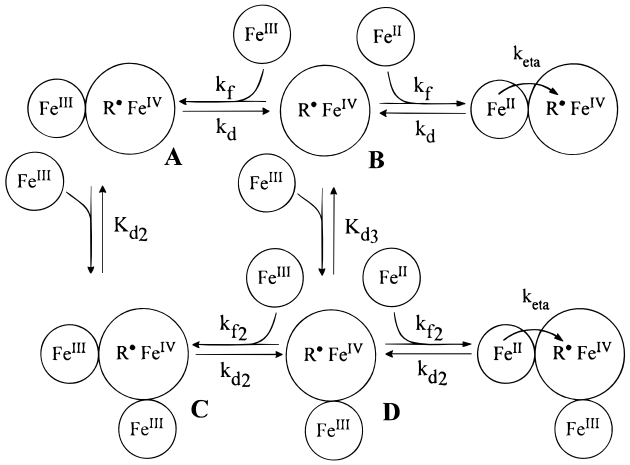

The kinetic data were analyzed using Scheme 3. Numerical integration methods were used to determine the observed rate constant k_{obs} obtained with a wide range of values for the rate constants in Scheme 3, as described in the supplementary material. These numerical integration methods confirmed that the steady-state eqs 1−3 were valid under the conditions specified. The experimental k_{obs} data were fitted by eqs 1−3 using the Marquardt−Levenberg nonlinear regression algorithm in SigmaPlot. The error for each parameter reported in the tables and figures is the asymptotic standard error representing 95% confidence limits given by the algorithm. The upper or lower limits for a parameter that is too small or too large to be measured is obtained from the standard errors (e.g., $k_d = 0.1 \pm 5.0$ indicates that $k_d < 5$). The Marquardt−Levenberg algorithm also gives parameter dependencies which indicate when too many parameters are used in the curve fitting process. It is assumed in Scheme 3 that the formation and dissociation rate constants k_f, k_d, k_{f2}, and k_{d2} are independent of the redox state of C*c*. The systematic error arising from this assumption appears to be less than a factor of two however, since McLendon et al. (1993) found that the equilibrium dissociation constant $K_d = k_d/k_f$ for the high-affinity binding site on MgC*c*P was the same for oxidized and reduced yC*c*, while Mauk et al. (1994) found that the dissociation constant for native C*c*P differed by only a factor of 2 for oxidized and reduced yC*c*.

RESULTS

Reaction between Ru-39-Cc^{II} and CMPI at Low Ionic Strength. Wang et al. (1996) showed that laser excitation of a 1:1 mixture of Ru-39-C*c* and CMPI at low ionic strength results in rapid electron transfer from Ru^{II*} to heme c, followed by electron transfer from heme c Fe^{II} to the Trp-

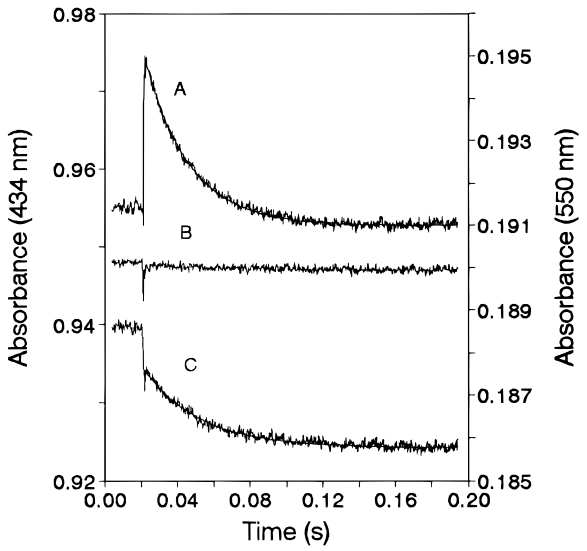

FIGURE 1: Photoinduced electron transfer reaction from Ru-39-Cc^{II} to CMPI in the presence of yCc^{III}. The solution contained 5 μM Ru-39-Cc, 5 μM yCc^{III}, and 5 μM CMPI in 1 mM sodium phosphate, pH 7, 2 mM aniline, at 25 °C. A light flash from the dye laser was used to photoreduce about 0.5 μM Ru-39-Cc, which transferred an electron to CMPI. (A) The slow phase of the 550 nm transient. The pseudo-first-order rate constant is $k_{obs} = 41 \pm 5$ s^{-1}. The fast phase due to rapid intracomplex electron transfer from Ru-39-Cc^{II} to the radical cation within the high-affinity Ru-39-Cc^{II}:CMPI complex was not resolved on this time scale. (B) The 434 nm transient under the same conditions as A. No absorbance change was observed, which indicated that the Trp-191 radical cation was reduced rather than the oxyferryl heme. (C) The solution in A was subjected to a series of light flashes to reduce the radical in CMPI, and then an additional flash was used to measure the reduction of the oxyferryl heme in CMPII at 434 nm. The fast phase in the 434 nm transient, corresponding to the sudden drop in absorbance, has a first-order rate constant of 5000 s^{-1}. The slow phase of the 434 nm transient has a pseudo-first-order rate constant of $k_{obs} = 41 \pm 6$ s^{-1}.

191 radical cation in CMPI with a rate constant of $k_{eta} = 2 \times 10^6$ s^{-1}. The rate constant is independent of protein concentration, provided that the CMPI concentration is equal to or greater than that of Ru-39-Cc. This observation indicates that k_{eta} describes electron transfer within the high-affinity 1:1 complex between Ru-39-Cc and CMPI, which has a dissociation constant K_d of <0.1 μM (Wang et al., 1996). To investigate the role of the second, low-affinity Cc binding site, the reaction of photoreduced Ru-39-Cc with CMPI was studied in the presence of excess oxidized wild-type yCc^{III}. The laser intensity in these experiments was set to photoreduce only about 5% of the Ru-39-Cc molecules in a single flash, so oxidized Ru-39-Cc^{III}, yCc^{III}, and CMPI were present in large excess over reduced Ru-39-Cc^{II}. Photoexcitation of a solution containing 5 μM Ru-39-Cc^{III}, 5 μM yCc^{III}, and 5 μM CMPI in 2 mM sodium phosphate, pH 7.0, resulted in two phases, a fast phase with rate constant $k_{eta} = 2.0 \times 10^6$ s^{-1}, and a very slow phase with rate constant $k_{obs} = 41 \pm 6$ s^{-1} (Figure 1A). The fast phase was assigned to intracomplex electron transfer from photoreduced Ru-39-Cc^{II} to the radical cation in the high-affinity Ru-39-Cc^{II}:CMPI complex. The slow phase is due to the reaction of solution-phase Ru-39-Cc^{II}. No decrease in the 434 nm absorbance is associated with the slow phase (Figure 1B), indicating that this phase is due to electron transfer to the radical cation in CMPI rather than the oxyferryl heme. When the sample was subjected to a multiple flash series to reduce CMPI to CMPII, an additional flash initiated the reaction between reduced Ru-39-Cc^{II} and the oxyferryl heme in CMPII, as described by Geren et al. (1991). This protocol gave a fast phase with a rate constant of $k_{etb} = 5000$ s^{-1} due to reduction of the oxyferryl heme by Ru-39-Cc^{II} in the high-affinity site, and a slow phase due to reduction of the oxyferryl heme by solution-phase Ru-39-Cc^{II} (Figure 1C). The rate constant k_{obs} for this slow phase, 41 ± 6 s^{-1}, is the same as the slow phase k_{obs} measured for reduction of the radical cation in CMPI (Figure 1A). Given the large difference in intracomplex rate constants for reduction of the radical cation and the oxyferryl heme, it appears that k_{obs} is not due to direct electron transfer; instead the rate is limited by complex formation or dissociation.

As the concentration of yCc^{III} is increased, the amplitude of the fast phase due to intracomplex reduction of the radical in CMPI decreases and the amplitude of the slow phase increases, indicating that yCc^{III} competitively displaces Ru-39-Cc^{III} from the high-affinity binding site. Wang et al. (1996) have shown that Ru-39-Cc and yCc have the same affinity for the high-affinity binding site on CMPI. The rate constant of the slow phase, k_{obs}, decreases as the concentration of yCc^{III} increases (Figure 2). These results are consistent with Scheme 3, in which yCc can bind to the high-affinity site (shown on the left side of CMPI), and to a second low-affinity binding site (shown on the bottom of CMPI). The binding of yCc to the low-affinity site is postulated to increase the dissociation rate constant of the high-affinity site from k_d to k_{d2}. It is assumed that only the high-affinity binding site is active in electron transfer. At low ionic strength and excess Cc^{III}, nearly all of CMPI will be either in the 1:1 complex A with dissociation constant $K_d = k_d/k_f$ or in the 2:1 complex C with dissociation constant K_{d2}. When a small amount of Ru-39-Cc^{II} is produced by the flash, it must bind to the high-affinity site on either B or D to reduce the radical. Since k_{eta} is much larger than k_d or k_{d2}, the pseudo-first-order rate constant is $k_{obs} = k_f[B] + k_{f2}[D]$. Steady-state expressions for [B] and [D] were obtained assuming that $K_d < 0.1$ μM and $K_{d2} > 20$ μM:

$$[B] = \frac{k_d E_o/k_f}{(C_o - E_o)(1 + (C_o - E_o)/K_{d2})}$$

$$[D] = \frac{k_{d2} E_o/k_{f2}}{K_{d2} + C_o - E_o}$$

where C_o = total [yCc^{III}] and E_o = total [CMPI]. k_{obs} is thus given by

$$k_{obs} = \frac{k_d E_o}{(C_o - E_o)(1 + (C_o - E_o)/K_{d2})} + \frac{k_{d2} E_o}{K_{d2} + C_o - E_o} \quad (1)$$

k_{obs} does not depend on the values of the formation rate constants k_f and k_{f2} in Scheme 3 at low ionic strength, provided that they are greater than 10^9 M^{-1} s^{-1}. yCc^{III} will compete with Ru-39-Cc^{II} for binding to B and D, and thus decrease the concentrations of B and D and lower k_{obs}. Nonlinear regression of the experimental concentration dependence of k_{obs} using eq 1 resulted in $K_{d2} = 65 \pm 20$ μM, $k_{d2} = 600 \pm 200$ s^{-1}, and $k_d < 5$ s^{-1} (Figure 2). These results indicate that the binding of yCc^{III} to the second low-affinity site increases the dissociation rate constant of the high-affinity site from $k_d < 5$ s^{-1} to $k_{d2} = 600$ s^{-1}.

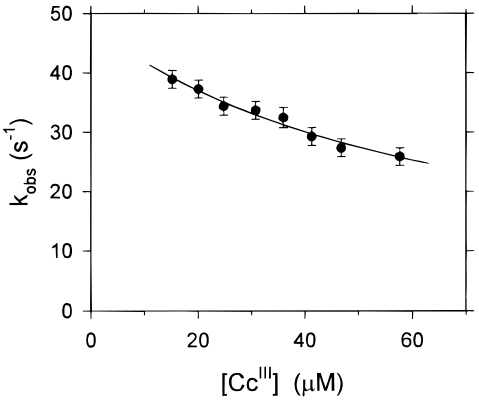

FIGURE 2: Effect of yCc^{III} concentration on the rate constant k_{obs} (in s^{-1}) for the slow phase of the reaction between Ru-39-Cc^{II} and CMPI. The experiment was carried out as described in Figure 1 with 5.0 μM Ru-39-C*c*, 5.0 μM CMPI, and 5−55 μM yCc^{III} in 2 mM sodium phosphate, pH 7.0, 2 mM aniline. The x axis gives the total concentration of both forms of Cc^{III}. The solid line is the nonlinear regression of eq 1 to the experimental data with k_{d2} = 600 ± 200 s^{-1}, K_{d2} = 65 ± 20 μM, and k_d < 5 s^{-1}.

Effect of Ionic Strength on the Reaction between Ru-39-Cc^{II} and CMPI. The effect of ionic strength on the slow phase of the reaction was studied in solutions containing 10 μM Ru-39-C*c* and 5 μM CMPI (Figure 3). k_{obs} increases from 40 s^{-1} at 5 mM ionic strength to a maximum of 2000 s^{-1} at 150 mM ionic strength and then decreases to 700 s^{-1} at 300 mM ionic strength. The initial increase in k_{obs} suggests that increasing ionic strength increases the dissociation rate constants k_d and/or k_{d2} for the high-affinity binding site. Regression analysis of the concentration dependence of k_{obs} at 44 mM ionic strength using eq 1 indicated that K_{d2} > 200 μM, and that it was not possible to determine the individual values of K_{d2} and k_{d2} for the low-affinity site. Therefore, since $K_{d2} \gg C_o$, eq 1 was modified to eq 2 which contains just two parameters:

$$k_{obs} = k_d E_o/(C_o - E_o) + (k_{d2}/K_{d2})E_o \qquad (2)$$

Regression analysis with eq 2 yielded k_d = 120 ± 20 s^{-1} and k_{d2}/K_{d2} = (6.2 ± 2) × 10^6 M^{-1} s^{-1} (Figure 4, Table 1). At ionic strengths above 60 mM the assumption that K_d < 0.1 μM may no longer be valid, and k_{obs} is given by eq 3, assuming K_{d2} > 200 μM, $k_{eta} \gg k_d$, and $k_{eta} \gg k_{d2}$:

$$k_{obs} = k_f\{E_o - 1/2(k_d/k_f + E_o + C_o - ((k_d/k_f + E_o + C_o)^2 - 4E_oC_o)^{1/2})\} + (k_{d2}/K_{d2})E_o \quad (3)$$

At 74 mM ionic strength, regression analysis using eq 3 indicated that k_d = 800 ± 200 s^{-1}, k_f > 3 × 10^9 M^{-1} s^{-1}, and k_{d2}/K_{d2} < 8 × 10^6 M^{-1} s^{-1} (Figure 5). Therefore, at ionic strengths of 74 mM and above the effect of the low-affinity binding site is no longer measurable, and the kinetics are described by the top line of Scheme 3. As the ionic strength is increased up to 104 mM, k_d increases to 1900 ± 300 s^{-1}, k_f = (3.0 ± 1.0) × 10^9 s^{-1}, and K_d = 0.6 ± 0.2 μM (Figure 5, Table 1). It was possible to measure k_d at ionic strengths from 40 to 150 mM, and k_f at ionic strengths from 100 to 300 mM (Figure 6, Table 1).

Effect of Surface Mutations of CcP on the Reaction with Ru-39-Cc. The effect of surface mutants of C*c*P on the reaction with excess Ru-39-C*c* was studied to define the binding domain (Figure 3). The mutants D34N and E290N had larger k_{obs} values at 2 mM ionic strength than C*c*P(MI),

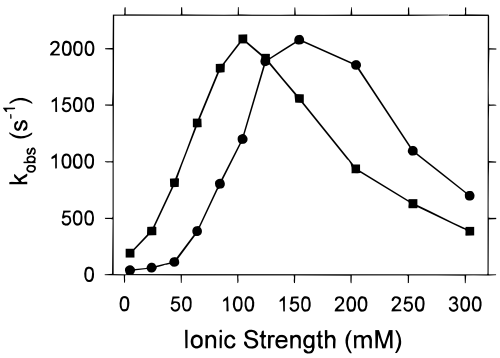

FIGURE 3: Effect of ionic strength on k_{obs} (in s^{-1}) for the reaction between Ru-39-Cc^{II} and CMPI in the presence of excess Ru-39-Cc^{III}. The reaction was carried out as described in Figure 1 with 10 μM Ru-39-C*c* and 4 μM CMPI, in 2 mM sodium phosphate, pH 7.0, 0 to 300 mM NaCl, and 2 mM aniline. (●) C*c*P(MI); (■) E290Q. The solid lines simply connect the points.

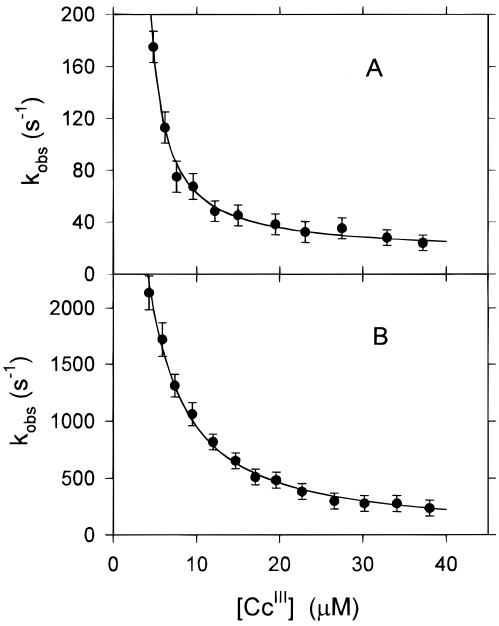

FIGURE 4: Effect of yCc^{III} concentration on k_{obs} (in s^{-1}) for the reaction between Ru-39-C*c* and CcP(MI) or D34N CMPI at 44 mM ionic strength. (A) The reaction was carried out with 2.5 μM Ru-39-C*c*, 2.6 μM CcP(MI) CMPI and 3 to 35 μM yCc^{III} in 2 mM sodium phosphate, pH 7.0, 40 mM NaCl. The solid line is the nonlinear regression of eq 2 to the experimental data with k_d = 120 ± 20 s^{-1} and k_{d2}/K_{d2} = (6.2 ± 2) × 10^6 M^{-1} s^{-1}. (B) The reaction was carried out with 2.5 μM Ru-39-C*c*, 2.6 μM D34N CMPI and 3−35 μM yCc^{III} in 2 mM sodium phosphate, pH 7.0, 40 mM NaCl. The solid line is the nonlinear regression for eq 3 with k_d = 3300 ± 400 s^{-1}, k_f = (2.6 ± 0.3) × 10^9 M^{-1} s^{-1}, and k_{d2}/K_{d2} < 5 × 10^6 M^{-1} s^{-1}.

and k_{obs} increased more rapidly as the ionic strength was increased (Figure 3). The maximum in k_{obs} was reached at a lower ionic strength than for C*c*P(MI), and then k_{obs} decreased as the ionic strength was increased to 300 mM. Concentration dependence studies indicated that the low-affinity binding site did not play a role in the kinetics of D34N at an ionic strength of 44 mM, and that the kinetic parameters of the high-affinity site are k_f = (2.6 ± 0.3) × 10^9 M^{-1} s^{-1}, k_d = 3300 ± 400 s^{-1}, and K_d = 1.3 ± 0.2 μM (Figure 4B, Table 1). The k_d values of D34N, E290N, A193F, E35Q, and E32Q were found to be 27-, 15-, 11-, 10-, and 3-fold larger than the C*c*P(MI) control, respectively, while E291Q was the same as the control (Table 1). As the ionic strength was increased to 100 mM, the k_d values of all the mutants increased, and both k_d and k_f could be measured

Table 1: Effect of Mutants on Complex Formation between Ru-39-C*c* and CMPI at 44 and 104 mM Ionic Strength[a]

	$I = 44$ mM	$I = 104$ mM		
mutant	k_d (10^2 s^{-1})	k_d (10^2 s^{-1})	k_f (10^9 M^{-1} s^{-1})	K_d (μM)
C*c*P(MI)	1.2 ± 0.2	19 ± 3	3.0 ± 1.0	0.6 ± 0.2
E32Q	3.6 ± 0.4	29 ± 4	3.2 ± 0.5	0.9 ± 0.2
D34N	33 ± 4	88 ± 12	0.7 ± 0.1	13 ± 2
E35Q	12 ± 3	28 ± 6	2.4 ± 0.4	1.2 ± 0.3
E290N	18 ± 2	98 ± 20	0.9 ± 0.1	11 ± 2
E291Q	1.3 ± 0.2	23 ± 4	3.0 ± 1.0	0.8 ± 0.3
A193F	13 ± 2	76 ± 20	1.5 ± 0.2	5.1 ± 1.0

[a] The values of k_f and k_d were measured in 2 mM sodium phosphate, pH 7.0, and 40 or 100 mM NaCl as described in the text.

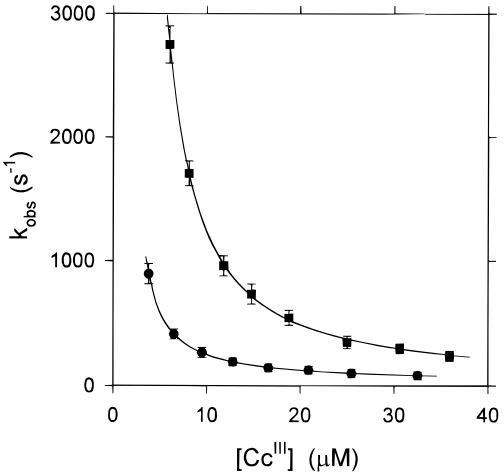

FIGURE 5: Effect of yCc^{III} concentration on k_{obs} for the reaction between Ru-39-C*c* and CMPI at 74 and 104 mM ionic strength. (●) 74 mM ionic strength. The reaction was carried out with 2.5 μM Ru-39-C*c*, 2.2 μM CMPI, and 2−30 μM yCc^{III} in 2 mM sodium phosphate, pH 7, 70 mM NaCl. The solid line is the nonlinear regression for eq 3 with $k_d = 800 \pm 200$ s^{-1}, $k_f > 3 \times 10^9$ M^{-1} s^{-1}, and $k_{d2}/K_{d2} < 8 \times 10^6$ M^{-1} s^{-1}. (■) 104 mM ionic strength. The reaction was carried out with 4 μM Ru-39-C*c*, 4.5 μM CMPI, and 2−30 μM yCc^{III} in 2 mM sodium phosphate, pH 7.0, 100 mM NaCl. The solid line is the nonlinear regression for eq 3 with $k_d = 1900 \pm 300$ s^{-1} and $k_f = (3 \pm 1) \times 10^9$ M^{-1} s^{-1}.

for the high-affinity site (Table 1). The k_f values of the D34N, E290N, and A193F mutants were smaller than that of C*c*P(MI), while the k_d and K_d values were larger (Table 1). The E32Q and E291Q mutants had nearly the same values of k_f, k_d, and K_d as the C*c*P(MI) control, while the kinetic constants for the E35Q mutant were intermediate (Table 1).

DISCUSSION

The yeast Ru-39-C*c* derivative satisfies two design criteria for the measurement of rapid interprotein electron transfer. First, there is an efficient pathway for electron transfer from Ru^{II*} to the heme group, and the rate constant is large, 5×10^5 s^{-1}. This allows the measurement of intracomplex electron transfer from Ru-39-Cc^{II} to the Trp-191 indolyl radical cation in CMPI and the oxyferryl heme in CMPII with rate constants of $k_{eta} = 2 \times 10^6$ s^{-1} and $k_{etb} = 5000$ s^{-1} (Wang et al., 1996). Second, the location of the ruthenium group on the back surface of Ru-39-C*c* was designed to allow normal interaction with C*c*P. The second-order rate constant k_a for the reaction of Ru-39-Cc^{II} with the radical in CMPI is the same as that for native yCc^{II} measured by stopped-flow spectroscopy over the ionic strength range from 150 to 600 mM (Wang et al., 1996). In addition, the dissociation

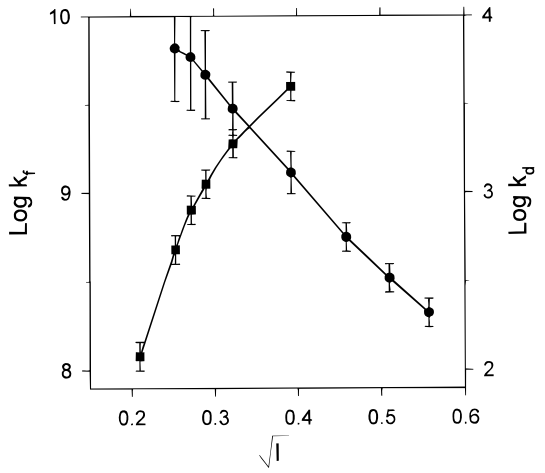

FIGURE 6: Dependence of the formation and dissociation rate constants for the Ru-39-C*c*:CMPI complex on ionic strength. The data were obtained as described in Figures 4 and 5 and fitted to eq 2 or 3 to obtain k_d (in s^{-1}) (■) and k_f (in M^{-1} s^{-1}) (●).

constant K_d for the high-affinity complex between Ru-39-C*c* and CMPI is the same as for native yC*c* at ionic strengths from 2 mM to 150 mM (Wang et al., 1996). These results provide strong evidence that the ruthenium complex on Ru-39-C*c* does not interfere with the interaction with CMPI.

To investigate the role of the low-affinity binding site, a technique was developed to measure the reaction of a small amount of photoreduced Ru-39-Cc^{II} with CMPI in the presence of excess yCc^{III}, as shown in Scheme 3. This technique has the advantage that the reaction involves the reduction of the Trp-191 radical cation in CMPI without the complicating effects of the reaction with the oxyferryl heme in CMPII (Figure 1). The intracomplex rate constant k_{eta} was found to be 2×10^6 s^{-1} under the same conditions used in the present experiments (Wang et al., 1996), which is much larger than k_d and is not rate-limiting for k_{obs}. This greatly simplifies kinetic analysis. The equilibrium dissociation constant K_{d2} obtained from the concentration dependence of k_{obs} at 4 mM ionic strength is 65 ± 20 μM, which is characteristic of the low-affinity binding site (Stemp & Hoffman, 1992; Matthis & Erman, 1995; Miller et al., 1996). However, k_{obs} does not involve direct electron transfer from Ru-39-Cc^{II} in the low-affinity binding site to the Trp-191 radical cation. The value of k_{obs} for electron transfer to the radical cation in CMPI is the same as for electron transfer to the oxyferryl heme in CMPII at the same protein concentrations (Figure 1). In contrast, the rate constants k_{eta} and k_{etb} for intracomplex electron transfer from Ru-39-Cc^{II} in the high-affinity site to the radical cation and the oxyferryl heme differ by 400-fold (Wang et al., 1996). Moreover, mesidine and related compounds also reduce the radical in CMPI more rapidly than the oxyferryl heme (Roe & Goodin, 1993), even though they react near the δ-meso edge of the heme on the opposite side from Trp-191 (Wilcox et al., 1996). Since the Trp-191 radical cation is reduced more rapidly than the oxyferryl heme regardless of the pathway for electron transfer, it appears that k_{obs} must be rate limited by complex dissociation rather than by an electron transfer step. It is proposed in Scheme 3 that the binding of yCc^{III} to the low-affinity binding site increases the rate constant for dissociation of yCc^{III} from the high-affinity binding site, allowing Ru-39-Cc^{II} to bind more rapidly to the high-affinity binding site and transfer an electron to the radical cation. The rate constant k_{d2} for dissociation of yCc^{III} from the high-

affinity binding site of the 2:1 complex was measured to be 600 ± 200 s^{-1} at 4 mM ionic strength. The rate constant k_d for dissociation of C*c*^{III} from the 1:1 complex was found to be less than 5 s^{-1} under the same conditions, consistent with the very strong binding of yC*c* to the high-affinity site (Kang et al., 1977). Scheme 3 is essentially the same as the "substrate-assisted product dissociation" mechanism proposed by Moench et al. (1992), McLendon et al. (1993), Corin et al. (1993), and Yi et al. (1994). A larger value for k_d, 180 s^{-1}, was estimated by Yi et al. (1994) in 10 mM KNO_3 using an NMR exchange technique, but this probably reflects the influence of the low-affinity site since protein concentrations larger than 250 μM were used. Miller (1996) has also found that k_d is very small, 5 s^{-1}, at 20 mM ionic strength.

It is of interest to compare our results on the low-affinity binding site with previous work. Pappa et al. (1996) cross-linked yC*c* to a putative low-affinity binding site at residue 149 of C*c*P. The rate constant for intracomplex electron transfer was very slow, 1 s^{-1}, and involved reduction of the radical cation rather than the oxyferryl heme, even though yC*c* was closer to the C*c*P heme than to Trp-191. Another cross-linked yC*c*−C*c*P complex was prepared to mimic the Pelletier−Kraut crystalline complex (Pappa et al., 1996). The turnover number of this complex with solution phase yC*c*^{II} was about 60 s^{-1} at low ionic strength, which is less than 10% of the value for native C*c*P. Wang and Margoliash (1995) found that a series of 1:1 cross-linked yC*c*−C*c*P complexes had turnover numbers with solution yC*c*^{II} ranging from 25 to 220 s^{-1} at low ionic strength. This large variation in activity presumably arises from different sites of covalent attachment of yC*c* on the C*c*P surface, but the location of these sites has not yet been reported. Miller et al. (1996) found that substitution of C*c*P Ala-193 with a bulky Cys-193-MPB group decreased the turnover number to 32 s^{-1}, independent of ionic strength. These results suggest that yC*c* was sterically constrained to bind to Cys-193-MPB-C*c*P with the orientation of the hC*c*:C*c*P complex rather than the yC*c*:C*c*P complex. Any direct electron transfer from the low-affinity site would have to be a small fraction of 32 s^{-1}. Zhou and Hoffman (1993, 1994) and Zhou et al. (1995) found that the rate of electron transfer from horse ^{3}ZnC*c* in the low-affinity site to the ferric heme in C*c*P was 1530 s^{-1} in the 2:1 ZnC*c*:C*c*P complex. The high-affinity C*c* binding site is inactive in this experiment because the Trp-191 indole is not oxidized to the radical cation, and the Pelletier−Kraut electron transfer pathway is inactive. In a related experiment, Stemp and Hoffman (1993) found that ^{3}ZnC*c*P transferred an electron to yC*c*^{III} in the 2:1 complex with a rate constant of about 60 s^{-1}, followed by reverse electron transfer from yC*c*^{II} to the Zn porphyrin radical in Zn^+C*c*P with a rate constant of about 3000 s^{-1}. Again, the low-affinity site was active in electron transfer, while the high-affinity site was inactive. The oxidation potential of the Zn-porphyrin radical is approximately 0.25 V lower than that of the oxyferryl heme, and will not be able to transiently oxidize the Trp-191 indole to the radical cation. This factor apparently inactivates the Pelletier−Kraut pathway to the high-affinity site. The low-affinity C*c* binding site must be close enough to the Zn-porphyrin in C*c*P to allow electron transfer by a different pathway not involving Trp-191. It is therefore of interest to question why the rate of electron transfer from yC*c*^{II} bound in the low-affinity site to the oxyferryl heme in CMPI is so slow. The reorganization energy for reduction of the oxyferryl heme is much larger than that for the ferric heme or the Zn-porphyrin radical due to the need to transfer protons to the oxygen atom and release the oxygen as water. This factor would significantly decrease the rate of reduction of the oxyferryl heme via the low-affinity site relative to that of the Zn-porphyrin radical. The redox properties and reorganization energy of the oxyferryl heme and Trp-191 indolyl radical cation therefore appear to favor electron transfer from the high-affinity site via the Pelletier−Kraut pathway, and prevent reduction via other less specific binding sites.

The low-affinity binding site does not play a significant role in the kinetics at ionic strengths above 70 mM (Figure 5). This is in agreement with the results of Mauk et al. (1994), who found that K_{d2} for the low-affinity site was 500 μM at 50 mM ionic strength, and even larger at higher ionic strength. The value of k_d increases from less than 5 s^{-1} at 2 mM ionic strength to 4000 s^{-1} at 150 mM ionic strength (Figure 6). This observation indicates that the high-affinity complex is stabilized by electrostatic interactions between charged residues on the surface of the complex that are sensitive to ionic shielding by solvent electrolyte (Kang et al., 1978). k_f decreases from greater than 3×10^9 M^{-1} s^{-1} at low ionic strength to 2.1×10^8 M^{-1} s^{-1} at 310 mM ionic strength, in good agreement with stopped-flow data for wild-type yC*c* (Wang et al., 1996). This result is consistent with Brownian dynamics simulations showing that electrostatic interactions facilitate translational and rotational diffusion leading to formation of the yC*c*:C*c*P complex (Northrup et al., 1988). The large value of k_f at low ionic strength is close to the diffusion limit for proteins of this size and charge distribution (Yi et al., 1994). The equilibrium dissociation constant of the high-affinity binding site, K_d, also increases significantly with increasing ionic strength, from $<10^{-8}$ M at 10 mM ionic strength (Kang et al., 1977) to 0.6 μM at 104 mM ionic strength in NaCl at pH 7 (Table 1). In comparison, Mauk et al. (1994) reported that $K_d = 2.8$ μM for the yC*c*:C*c*P complex at 100 mM ionic strength in KCl at pH 6.0, and estimated that it should be about 2-fold smaller at pH 7, in reasonable agreement with the present results.

The location of the high-affinity binding domain on C*c*P was investigated using surface mutants. The mutations D34N and E290N increased k_d 27-fold and 15-fold compared to the CMPI(MI) control at 44 mM ionic strength (Table 1). At 104 mM ionic strength, k_d was increased about 5-fold for each mutant compared to the control and k_f was decreased about 4-fold, leading to an approximately 18-fold increase in K_d (Table 1). Smaller effects were observed for the E35Q and E32Q mutations, while the E291Q mutation had essentially no effect. The relative effects of the charge mutations on k_d, k_f, and K_d parallel the location of these residues at the protein−protein interface of the crystalline yC*c*:C*c*P complex (Pelletier & Kraut, 1992). The terminal oxygen atoms of Asp-34 and Glu-290 are 3.8 and 3.2 Å from the amino groups of yC*c* lysines 87 and 73, respectively, which could allow significant electrostatic interactions at low ionic strength [see Figure 1 of Miller (1996)]. The carboxyl oxygens of Glu-35 and Glu-32 are more distant from the Lys-87 amino group on yC*c*, while the side chain of Glu-291 projects away from the interface with yC*c*. Mutation of Ala-193 at the center of the interaction domain to Phe results in a 11-fold increase in k_d at 44 mM ionic strength. The effects of these surface mutations on k_d parallel their effects on steady-state turnover at low ionic strength,

providing support for a mechanism in which complex dissociation is rate-limiting at low ionic strength (Miller, 1996). The effects of all the surface mutants on k_f, k_d, k_{eta}, k_{etb}, and steady-state turnover provide strong support for a mechanism in which the Pelletier−Kraut binding domain is used for reduction of both the Trp-191 indolyl radical cation and the oxyferryl heme.

CONCLUSIONS

The kinetic parameters needed for a complete description of the reduction of CMPI by two molecules of Cc^{II} as shown in Scheme 2 have been determined. Kinetic simulations using these parameters are in good agreement with experimental steady-state turnover rates over the ionic strength range 40 to 160 mM (Miller, 1996). The low-affinity binding site promotes product dissociation at low ionic strength but plays no role at physiological ionic strength. The rate constants in Scheme 2 at physiological ionic strength (150 mM) are $k_f = 1.3 \times 10^9$ s^{-1}, $k_d = 4000$ s^{-1}, $k_{eta} = 1.0 \times 10^6$ s^{-1}, and $k_{etb} = 3000$ s^{-1}. The value of the dissociation rate constant k_d is quite similar to the rate of intracomplex electron transfer to the oxyferryl heme, k_{etb}. Therefore, the rate-limiting step in enzyme turnover is product dissociation below 150 mM ionic strength, and intracomplex electron transfer to the oxyferryl heme above 150 mM ionic strength. The interaction between yC*c* and C*c*P is optimized at physiological ionic strength to provide the largest possible complex formation rate constant k_f, without allowing product dissociation to be rate-limiting. The binding domain identified in the crystalline yC*c*:C*c*P complex is used for reduction of both the Trp-191 radical cation and the oxyferryl heme at all ionic strengths.

ACKNOWLEDGMENT

We thank Dr. Mark A. Miller for a generous gift of the C*c*P(MI) mutants used in this study, and for enlightening discussions on this work.

SUPPORTING INFORMATION AVAILABLE

Steady-state equations for and numerical integration of Scheme 3 (3 pages). Ordering information is given on any current masthead page.

REFERENCES

Corin, A. F., Hake, R. A., McLendon, G., Hazzard, J. T., & Tollin, G. (1993) *Biochemistry 32*, 2756−2762.

Coulson, A. F. W., Erman, J. E., & Yonetani, T. (1971) *J. Biol. Chem. 246*, 917−924

Edwards, S. L., Xuong, N. H., Hamlin, R. C., & Kraut, J. (1987) *Biochemistry 26*, 1503−1511.

Erman, J. E., Vitello, L. B., Mauro, J. M., & Kraut, J. (1989) *Biochemistry 28*, 7992−7995.

Fishel, L. A., Villafranca, J. E., Mauro, J. M., & Kraut, J. (1987) *Biochemistry 26*, 351−360.

Fitzgerald, M. M., Churchill, M. J., McRee, D. E., & Goodin, D. B. (1994) *Biochemistry 33*, 3807−3818.

Fulop, V., Phizackerley, R. P., Soltis, S. M., Clifton, F. J., Wakatsuki, S., Erman, J., Hajdu, J., Edwards, S. L., (1994) *Structure 2*, 201−208.

Geren, L. M., Hahm, S., Durham, B., & Millett, F. (1991) *Biochemistry 30*, 9450−9457

Geren, L. M., Beasley, J. R., Fine, B. R., Saunders, A., Hibdon, S., Pielak, G. J., Durham, B., and Millett, F. (1995) *J. Biol. Chem. 270*, 2466−2472.

Hahm, S., Durham, B., & Millett, F. (1992) *Biochemistry 31*, 3472−3477.

Hahm, S., Geren, L., Durham, B., & Millett, F. (1993) *J. Am. Chem. Soc. 115*, 3372−3373.

Hahm, S., Miller, M. A., Geren, L., Kraut, J., Durham, B., & Millett, F. (1994) *Biochemistry 33* 1473−1480.

Huyett, J. E., Doan, P. E., Gurbiel, R., Houseman, A. L. P., Sivaraja, M., Goodin, D. B., & Hoffman, B. M. (1995) *J. Am. Chem. Soc. 117* 9033−9041.

Kang, C. H., Ferguson-Miller, S., & Margoliash, E. (1977) *J. Biol. Chem. 252* 919−926.

Kang, C. H., Brautigan, D. L., Osheroff, N., & Margoliash, E. (1978) *J. Biol. Chem. 253*, 6502−6510.

Kornblatt, J. A., & English, A. M. (1986) *Eur. J. Biochem. 155* 505−511.

Liu, R.-Q., Hahm, S., Miller, M. A., Han, G. W., Geren, L., Hibdon, S., Kraut, J., Durham, B., & Millett, F. (1994) *Biochemistry 33* 8678−8685.

Liu, R.-Q., Hahm, S., Miller, M., Durham, B., & Millett, F. (1995) *Biochemistry 34* 973−983.

Matthis, A. L., & Erman, J. E. (1995) *Biochemistry 34* 9985−9990.

Matthis, A. L., Vitello, L. B., & Erman, J. E. (1995) *Biochemistry 34*, 9991−9999.

Mauk, M. R., Ferrer, J. C., & Mauk, A. G. (1994) *Biochemistry 33* 12609−12614.

Mauro, J. M., Fishel, L. A., Hazzard, J. T., Meyer, T. E., Tollin, G., Cusanovich, M. A., & Kraut, J. (1988) *Biochemistry 27* 6243−6256.

McLendon, G., Zhang, Q., Wallin, S. A., Miller, R. M., Billstone, V., Spears, K. G., & Hoffman, B. M. (1993) *J. Am. Chem. Soc. 115* 3665−3669.

Miller, M. A. (1996) *Biochemistry 35*, 15791−15799.

Miller, M. A., Han, G. W., & Kraut, J. (1994a) *Proc. Nat. Acad. Sci. USA 91* 11118−11122.

Miller, M. A., Liu, R.-Q., Hahm, S., Geren, L., Hibdon, S. Kraut, J., Durham, B., & Millett, F. (1994b) *Biochemistry 33* 8686−8693.

Miller, M. A., Erman, J. E., & Vitello, L. B. (1995) *Biochemistry 34* 12048−12058.

Miller, M. A., Geren, L., Han, G. W., Saunders, A., Beasley, J., Pielak, G. J., Durham, B., Millett, F., & Kraut, J. (1996) *Biochemistry 35* 667−673.

Moench, S., Chroni, S., Lou, B. S., Erman, J., & Satterlee, J. (1992) *Biochemistry 31*, 3661−3670.

Northrup, S. H., Boles, J. O., & Reynolds, J. C. L. (1988) *Science 241*, 67−70.

Pappa, H. S., Tajbaksh, S., Saunders, A. J., Pielak, G. J., Poulos, T. L. (1996) *Biochemistry 35* 4837−4845.

Pelletier, H., & Kraut, J. (1992) *Science 258* 1748−1755.

Roe, J. A., & Goodin, D. B. (1993) *J. Biol. Chem. 268* 20037−20045.

Scholes, C. P., Liu, Y., Fishel, L. A., Farnum, M. F., Mauro, J. M., & Kraut, J. (1989) *Isr. J. Chem. 29* 85−92.

Sivaraja, M., Goodin, D. B., Smith, M., & Hoffman, B. M. (1989) *Science 245* 738−740

Stemp, E. D. A., & Hoffman, B. M. (1993) *Biochemistry 32* 10848−10865.

Wang, K. F., Mei, H. K., Geren, L., Miller, M. A., Saunders, A., Wang, X., Pielak, G. J., Durham, B., & Millett, F. (1996) *Biochemistry* (in press).

Wang, Y., & Margoliash, E. (1995) *Biochemistry 34*, 1948−1958.

Wilcox, S. K., Jensen, G. M., Fitzgerald, M. M., McRee, D. E., & Goodin, D. B. (1996) *Biochemistry 35* 4858−4866.

Yi, Q., Erman, J. E., & Satterlee, J. D. (1994) *J. Am. Chem. Soc. 116* 1981−1987.

Zhou, J. S., & Hoffman, B. M. (1993) *J. Am. Chem. Soc. 113* 11008−11009.

Zhou, J. S., & Hoffman, B. M. (1994) *Science 265* 1693−1696.

Zhou, J. S., Nocek, J. M., De Van, M. L., & Hoffman, B. M. (1995) *Science 269* 204−207.

BI961487K